Experiments in Fluids (2006) 41: 147–153
DOI 10.1007/s00348-005-0080-y

RESEARCH ARTICLE

**Philippe Marmottant · Michel Versluis · Nico de Jong
Sascha Hilgenfeldt · Detlef Lohse**

High-speed imaging of an ultrasound-driven bubble in contact with a wall: "Narcissus" effect and resolved acoustic streaming

Received: 4 July 2005 / Revised: 25 October 2005 / Accepted: 26 October 2005 / Published online: 8 December 2005

Abstract We report microscopic observations of the primary flow oscillation of an acoustically driven bubble in contact with a wall, captured with the ultra high-speed camera Brandaris 128 (Chin et al. 2003). The driving frequency is up to 200 kHz, and the imaging frequency is up to 25 MHz. The details of the bubble motion during an ultrasound cycle are thus resolved, showing a combination of two modes of oscillations: a radius oscillation and a translation oscillation, perpendicular to the wall. This motion is interpreted using the theory of acoustic images to account for the presence of the wall. We conclude that the bubble is subjected to a periodic succession of attractive and repulsive forces, exerted by its own image. Fast-framing recordings of a tracer particle embedded in the liquid around the particle are performed. They fully resolve the acoustic streaming flow induced by the bubble oscillations. This non-linear secondary flow appears as a tiny drift of the particle position cycle after cycle, on top of the primary back and forth oscillation. The high oscillation frequency accounts for a fast average particle velocity, with characteristic timescales in the millisecond range at the lengthscale of the bubble. The features of the bubble motion being resolved, we can apply the acoustic streaming theory near a wall, which provides predictions in agreement with the observed streaming velocity.

P. Marmottant (✉) · M. Versluis · N. de Jong · S. Hilgenfeldt
D. Lohse
Department of Science and Technology, University of Twente,
P.O. Box 217, 7500 Enschede, The Netherlands
E-mail: philippe.marmottant@ujf-grenoble.fr

N. de Jong
Department of Experimental Echocardiography, Thoraxcentre,
Erasmus MC, Rotterdam, The Netherlands

Present address: P. Marmottant
Laboratoire de Spectrométrie Physique, CNRS-Université Joseph
Fourier, BP 87, 38402 Saint Martin d'Hères, France

Present address: S. Hilgenfeldt
Engineering Sciences & Applied Mathematics and Department
of Mechanical Engineering, Northwestern University,
2145 Sheridan Road, Evanston, IL 60208, USA

1 Introduction

Looking in a mirror, Narcissus was irresistibly attracted by his image, according to Greek mythology. In this article, we will see that a bubble oscillating in liquid on a wall displays an attraction as well, creating an oscillatory translating motion of the bubble.

The interest in bubble oscillations in the vicinity of a wall has been raised by the use of micrometric bubbles as contrast agents for ultrasound echography (Klibanov 2002). In addition to an improvement in the quality of images, sonoporation treatment—that is the acoustic permeabilization of lipidic membranes—is strongly enhanced by the presence of microbubbles near cell walls (Tachibana et al. 1999; Miller and Quddus 2000; Ward et al. 2000). This provides a new avenue for localized drug delivery and gene transfer into cells using microbubbles and focused ultrasound. Close microscopic observations revealed strong streaming currents around microbubbles in contact with a wall (Marmottant and Hilgenfeldt 2003), with large velocity gradients leading to the rupture of the membranes of lipid vesicles. These observations provide a possible sonoporation mechanism.

Acoustic streaming, a secondary non-linear effect, is at the origin of the steady flow around the bubble. Indeed, secondary steady streamlines were theoretically predicted near a wall (Marmottant and Hilgenfeldt 2003) assuming a combination of primary oscillations: a volume oscillation together with an oscillation of the center of mass perpendicular to the wall, extending the calculations of Longuet-Higgins (1998) for a bubble in bulk. The translation may be driven by the fluctuating buoyancy force for a bubble in the bulk (Longuet-Higgins 1997), while the cause of the translation near a boundary is not documented. Although not directly observed, a phase shift between the two kinds of oscillations was theoretically found to be necessary to drive the microstreaming.

The purpose of this study is to image the primary bubble oscillation at the ultrasound frequency, as well as the primary motion of the surrounding fluid. We also propose a theoretical description to account for the primary oscillations and the non-zero phase shift.

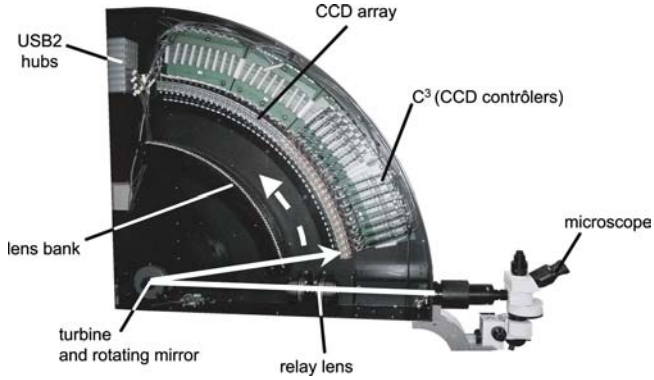

Fig. 2 Photograph of the fast-framing camera Brandaris 128 (Chin et al. 2003). The image from the microscope is successively projected on 128 CCD cameras by the rotating mirror

2 Methods

2.1 Acoustic excitation of the microbubble

An air bubble (10–100 μm in radius) is fixed by capillarity to the wall of a quartz cuvette (Hellma, Germany, 10 mm×10 mm×45 mm). It is introduced by injecting air in the cuvette with a syringe (see Fig. 1). Mixtures of water and glycerol allow to increase the liquid viscosity compared to that of pure water, with a kinematic viscosity of up to 6.8 times that of water.

A piezo-electric transducer (1 mm thick; PIC 151 ceramic from Physik Instrumente, Germany) glued to the wall generates ultrasonic vibrations (20–200 kHz) upon excitation. The excitation amplitude remains constant, resulting in a standing ultrasound field in the liquid inside the cuvette, with millimetric wavelengths much larger than the bubble size. The typical sound amplitude, inferred from the measured bubble vibration amplitude, is $P_{ac} \lessapprox 0.1$ bar.

Side view and bottom views of the bubble through the quartz are obtained using a bright field microscope (Olympus modular BX2, Japan).

2.2 Image acquisition with the ultrafast-framing camera Brandaris 128

In order to fully resolve the bubble oscillation with a camera, the acquisition rate must be higher than the ultrasound frequency (the latter being 200 kHz at maximum). We used for that purpose the fast-framing camera Brandaris 128 that records a sequence of 128 images with up to 25 million frames per second. The description of the camera, detailed in Chin et al. (2003), is summarized here, following the path of light from the beginning: a short arc xenon flash lamp (EG&G FX-1163 Perkin-Elmer Optoelectronics, Salem, MA, USA) produces a flash of a few microsecond in duration to illuminate the bubble scene during the recording, the upright microscope sends a 40× magnified image to the camera (see Fig. 2). The image is directed by relay lenses on a rotating mirror driven by a turbine, which redirects the image on the array of CCD cameras, arranged along an arc. The successive illumination of the CCD provides a sequence of 128 static images. The interframe time depends on the adjustable rotation rate of the mirror, allowing the maximum of 25 million frames per second.

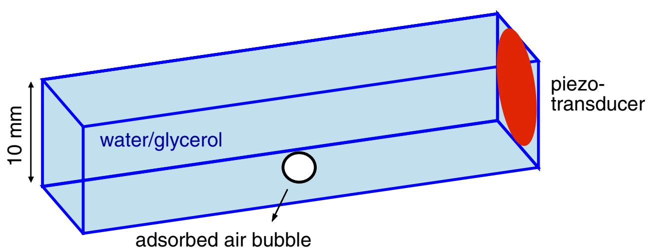

Fig. 1 The air microbubble is sticking on the wall of a cuvette due to capillarity. A piezo-transducer generates a standing ultrasound wavefield within the cuvette, exciting bubble vibrations

2.3 Image analysis

The image sequence of the oscillating bubble is automatically analyzed to measure the bubble volume and the position of the bubble center (see an example, Fig. 3, left). For that purpose, a circle is superimposed to the image contour, assuming that the bubble remains spherical.

Since recorded images show only a part of the circular boundary, we developed a specific algorithm to monitor the boundary center and radius automatically. The algorithm proceeds as follows:

- A gradient filter is applied to enhance the edges (a Sobel filter, see Fig. 3, right).
- The image is convoluted with a series of computer-generated images of a circle, with a range of radii (using Fast Fourier Transforms).
- The measured bubble radius is the one of the circle that provides the highest correlation. The position of the peak in the correlation image provides the center of the bubble.

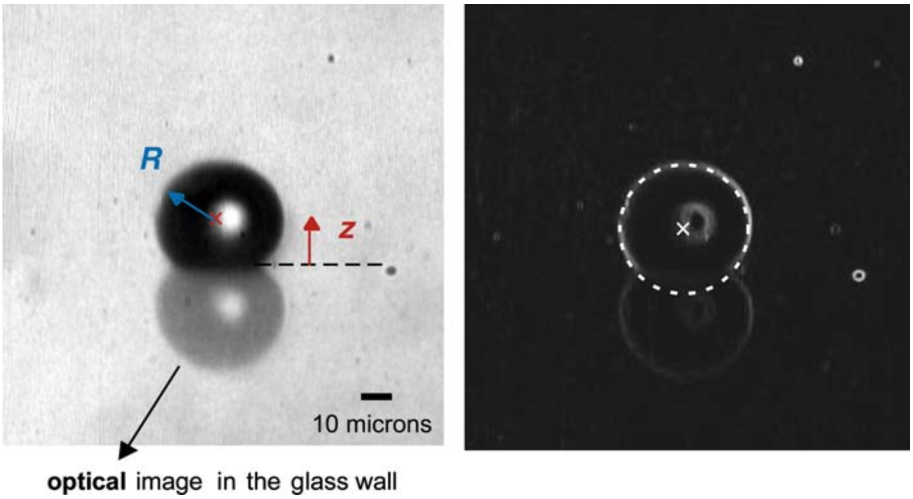

Fig. 3 Air microbubble, 20 μm in radius, side view (*left*). The reflection on the glass provides the optical image. Contour and center recognition on the gradient image (*right*)

3 Bubble translation oscillation

Looking from the side, tangentially to the glass wall (see Fig. 3, left), the elevation of the center of mass z and the radius of the bubble R are measured simultaneously. The analysis of a fast-framing sequence reveals that the center of mass translates away and towards the wall during the volume oscillation, around an average position z_0 (see a cycle, Fig. 4). While the translation and radius oscillation occur at the same frequency, they are not in phase. The examination of individual images shows that the bubble shape remains quasi spherical during the oscillation (low surface undulation modes).

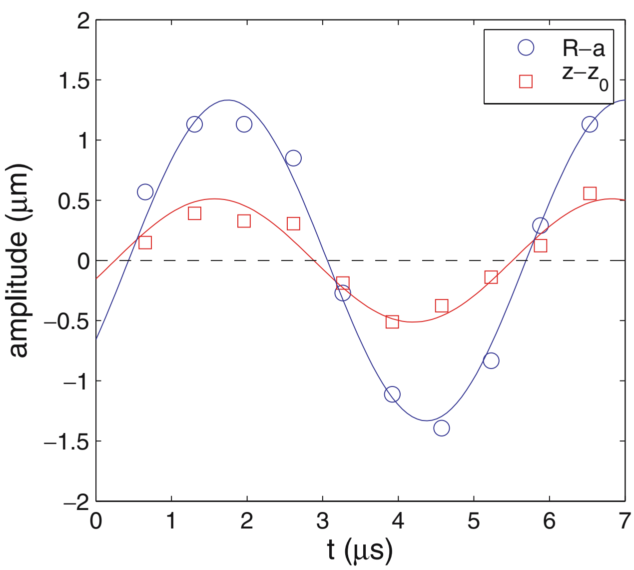

Fig. 4 Measurements from the images (recorded at the rate of 1,500,000 frames per second): the bubble radius R and the center of mass z are out of phase ($\Delta\phi = -13°$), and oscillate with the ultrasound frequency of 191 kHz

We perform an harmonic fit of the measured oscillations with

$$R(t) = a(1 + \epsilon' \exp(\mathrm{i}\omega t)), \tag{1}$$
$$z(t) = z_0 + a\epsilon \exp(\mathrm{i}\omega t - \mathrm{i}\Delta\phi), \tag{2}$$

using the complex notation, with a the bubble radius at rest, ε' the normalized amplitude of the radius oscillation, ε the amplitude of the translation oscillation, $\omega = 2\pi f$ the angular pulsation frequency, $\Delta\phi$ the phase shift between the oscillation. It is important to note here that we follow the notation from Longuet-Higgins (1998), except for the definition of the phase shift $\Delta\phi$ that differs by an angle of π with the phase shift ϕ defined in that reference, with $\Delta\phi = \phi - \pi$.

Considering the three cycles of best illumination, we find that the bubble ($a = 20$ μm) oscillates at the driving acoustic frequency ($f = 191$ kHz). The oscillation amplitude is $\varepsilon' = 0.077$, and the translation amplitude is $\varepsilon = 0.35\varepsilon'$. In spite of the limited accuracy of the measurement, a clear negative phase shift is measured, $\Delta\phi = -13°$ (with a standard deviation of 7°), meaning that the translation precedes the volume oscillation.

Several hypotheses for the origin of the force driving the translation were initially considered by the authors, and we review them here: (1) A pinned contact, together with a fixed contact angle, could geometrically force an elevation increase during the inflation of the spherical bubble; however, this would not trigger any phase shift. (2) Ellipsoidal surface deformations around the spherical shape, driven by the surface tension force restoring the contact angle are not observed in experiments. (3) When taking a moving contact line into account an estimate shows no significant phase lag either, even in the case of stick–slip discontinuities (calculations not presented here). More generally, all capillary pressures due to the distortion of the interface are of order $\sigma\varepsilon'/a$, according to the Laplace law, with σ the surface tension, and negligible compared to inertial pressures which are according to Bernoulli's law of order $\rho_l(a\omega)^2$, with ρ_l the density of the liquid: the ratio of the inertial to capillary pressures defines a Weber number that is large, $We = \rho_l a^3 \omega^2 \varepsilon' / \sigma \simeq 15 \gg 1$.

The buoyancy force due to hydrostatic pressure gradients, candidate for the driving, is negligible for micrometric bubbles. Calculations show that inhomogeneities of the standing acoustic pressure field, creating gradients along the acoustic wavelength, much larger than the bubble size, do not contribute significantly either.

By contrast, the presence of the wall itself leads to a significant alternating pressure gradient. The pressure field is obtained from the flow field using the Navier–Stokes equation. The bubble wall velocities induced by the motion at the ultrasound frequency, with translational velocities of order $u_t \sim \varepsilon\ a\omega$ and radial velocities of order $u_r \sim \varepsilon'\ a\omega$, providing two Reynolds numbers: a translational Reynolds number $Re_t = R\ u_t/\nu = \varepsilon\ a^2\omega/\nu$, and a radial Reynolds number $Re_r = Ru_r/\nu = \varepsilon'\ a^2\omega/\nu$. From the previous measurements both Reynolds numbers are larger than 1 ($Re_t \simeq 2$ and $Re_r \simeq 6$), and we will use a high Reynolds number formalism as a first approximation. The pressure can therefore be derived from the potential flow theory for the primary motion of the fluid at the ultrasound frequency, neglecting the viscous effects localized in thin boundary layers at the walls.

The flow field near the wall can be modeled, in a first approximation, by replacing the wall by an *acoustic image* located symmetrically on the other side of the wall, *at the same position of the optical image* seen on the photographs, in order to satisfy a vanishing normal velocity at the wall. The interaction of a bubble with its own image was studied in literature within various contexts: in particular for the case of non-oscillating bubbles in translation parallel to a wall (Takemura and Magnaudet 2003), or in general translation near a wall (Magnaudet 2003). The phenomenon of acoustic streamers also triggered investigation on the interaction of oscillating bubble pairs, similar to the bubble–image pair when radii are equal (Pelekasis et al. 2004).

We have seen that acoustic forces from the pressure gradients of the ultrasound field in the cuvette, called primary Bjerknes forces (Leighton 1994; Brennen 1995), can be safely neglected. On the other hand, the oscillation of the acoustic image creates an alternating pressure gradient on the real bubble, resulting in an alternating secondary Bjerknes force (Leighton 1994; Brennen 1995). The force scales like $F_B \sim -V_B((\partial p_2)/(\partial r))$, where V_B is the bubble volume and p_2 is the emitted oscillating pressure from the acoustic image. At a distance r from the acoustic image this pressure scales like $p_2 \sim \rho_l R^2 \ddot{R}/r$, resulting in a secondary Bjerknes force $F_B \sim V_B \rho_l R^2 \ddot{R}/r^2$, directed away from the wall and proportional to the bubble wall acceleration. The bubble is therefore alternately *attracted and repelled by its own acoustic image*. Attraction occurs during the inward acceleration of the bubble wall, while repulsion occurs during the outward acceleration (see illustration, Fig. 5).

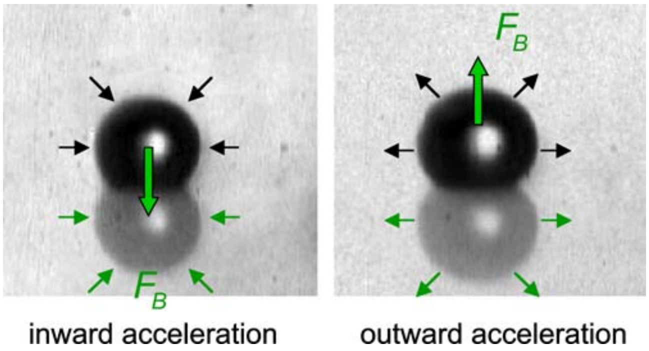

Fig. 5 Oscillating bubble at the end of the contraction phase (*left*), and at the end of expansion phase (*right*). The secondary Bjerknes force F_B by the *acoustic* image of the bubble produces alternately an attraction and a repulsion

According to van der Geld (2002) the velocity potential of an oscillating bubble near a wall can be expressed analytically as a sum of multipoles whose amplitude is determined by boundary conditions. The total kinetic energy is derived from the velocity potential, and the forces on the bubble are obtained from the Lagrange equation for the kinetic energy (the expression of the pressure field is therefore not needed within this method). At first order in $\varepsilon' \ll 1$ [linearizing equations from van der Geld (2002) for small vibration amplitudes], and considering a bubble far from the wall [$R/z \ll 1$, keeping terms up to $(R/z)^2$], the following inertial force components on the z axis are obtained: the added mass force

$$F_M = -C_M \rho_l V_B \ddot{z},$$

due to the acceleration of the fluid, with the added mass coefficient $C_M = 1/2$; and the secondary Bjerknes acoustic force

$$F_B = \frac{3}{4}\left(\frac{R}{z}\right)^2 \frac{1}{2} \rho_l V_B \ddot{R}. \quad (3)$$

Dissipative forces are the translation drag force and the expansion drag force, the latter being caused by the vicinity of the image bubble. Still following the results by van der Geld (2002) expressed for small vibration amplitudes and up to order $(R/z)^2$, we find that the drag force writes

$$F_D = -C_D \frac{1}{2} \rho_l \pi R^2 \dot{z}^2 = -12\pi\rho_l \nu R \dot{z}, \quad (4)$$

the drag coefficient being $C_D \simeq 24/Re_t$ at large Re_t number (see the review of Magnaudet and Eames 2000). Magnaudet and Legendre (1998) showed that expression 4 holds when at least one of the translation and radial Reynolds numbers is large, that is for $Re_t \gg 1$ or $Re_r \gg 1$. For the case where both Reynolds number are small, $Re_t \ll 1$ and $Re_r \ll 1$, the drag force writes

$$F_D = -4\pi\rho_l \nu R\dot{z} - 8\pi\nu \int_0^t \exp\left(\frac{9\nu\tau}{a^2}\right) \mathrm{erfc}\left(\sqrt{\frac{9\nu\tau}{a^2}}\right) R\ddot{z}(\tau)\,\mathrm{d}\tau, \tag{5}$$

the second term being the history force, here with a linearized expression at small vibration amplitudes. In the present situation both Reynolds numbers are not in the small number range: in our model calculations we will therefore employ the high Reynolds number expression 4, keeping in mind that we are in an intermediate region where low Reynolds number effects start to play a role.

The other dissipative force is the expansion drag force

$$F_E = -\frac{1}{2}\left(\frac{R}{z}\right)^2 12\pi\rho_l \nu R\dot{R}.$$

For bubbles close to the wall, the coefficients of all these forces slightly increase when $z/R \simeq 1$ (all with the same factor, within a few % when $z/R = 1.05$), but are not valid when the bubble is just above or in contact with the wall, as in the experiment. Exact calculations were presented for bubbles in contact with the wall (van der Geld 2004), but only for the inertial forces F_M and F_B: evaluating the dissipation in the thin films between the bubbles or within the corners near the contact line would require a complex description of the interplay between surface deformations and friction forces. Note that the translation and expansion drag forces F_D and F_E are likely to diminish at contact, when the liquid film between the bubbles disappears. We will therefore use the far field expression as a first order approximation, neglecting the effects of the contact line. From Newton's second law $F_M + F_B + F_D + F_E = 0$, we obtain

$$\ddot{z} + \frac{18\nu}{R^2}\dot{z} = \frac{3}{4}\left(\frac{R}{z}\right)^2 \ddot{R} - \left(\frac{R}{z}\right)^2 \frac{9\nu}{R^2}\dot{R}. \tag{6}$$

The response of the bubble elevation z to oscillations of the secondary Bjerknes force is formally analogous to the forced response of a dashpot. The first term on the right-hand side of Eq. 6 is a forcing introduced by the presence of the wall.

As a parenthesis, note that the radial dynamics is also affected by the acoustic image bubble. In linear approximation $R - R_0 \ll R_0$ (i.e., for $P_{ac}(t) < P_0$), the standard Rayleigh–Plesset equation, describing the radius response as a function of the acoustic pressure, becomes near a wall

$$\left(1 + \frac{1}{2}\frac{R}{z}\right)\ddot{R} + \frac{4\nu}{R^2}\dot{R} + \frac{P_0 - p_g(R) - \frac{2\sigma}{R}}{\rho R} = -\frac{P_{ac}(t)}{\rho R} + \frac{1}{8}\left(\frac{R}{z}\right)^2 \ddot{z} + \frac{3}{2}\left(\frac{R}{z}\right)^2 \frac{\nu}{R^2}\dot{z}, \tag{7}$$

using the far-field expression from van der Geld (2002) up to $\mathcal{O}((R/z)^2)$, with P_0 the ambient pressure, $p_g(R)$ the gas pressure in the bubble, and $P_{ac}(t)$ the applied acoustic pressure. The radius response is analogous to the forced response of an harmonic oscillator. We infer from the prefactor of the first term that the "mass" of the harmonic oscillator is increased by the presence of the wall, decreasing the resonance frequency. The acoustic pressure provides the forcing, and the oscillator is weakly coupled to the translational motion through the last two terms. We cannot measure the local acoustic pressure in the experiment and we will not elaborate further on the radial response to the acoustic pressure and just conclude that the acoustic image modifies the resonance properties of the bubble.

Inserting harmonic oscillations of R and z as described by Eqs. 1 and 2 in the translational equation 6, we obtain the following phase shift and amplitude response for the translation with respect to the radius oscillation:

$$\Delta\phi \simeq -\arctan\left(\frac{18\nu}{\omega R^2}\right) - \arctan\left(\frac{12\nu}{\omega R^2}\right), \tag{8}$$

$$\epsilon \simeq \epsilon' \frac{3}{4}\left(\frac{R}{z}\right)^2 \sqrt{\frac{1 + \left(\frac{12\nu}{\omega R^2}\right)^2}{1 + \left(\frac{18\nu}{\omega R^2}\right)^2}}. \tag{9}$$

The translation is indeed *in advance* with respect to radius oscillations (negative phase shift). The translation drag force accounts for the majority of the phase shift, and the expansion drag force for a small part of it. The phase shift is an increasing function of the viscosity of the liquid, and all the more pronounced for small bubbles. The amplitude of translation ε decays rapidly for increasing bubble to wall distances.

Predictions with the conditions of the experiment ($\nu = 6.8\times10^{-6}\mathrm{m}^2/\mathrm{s}$, $f = 191$ kHz, $R = 19.6$ µm, $R/z \simeq 1$) provide $\Delta\phi = -25°$, overestimating the experimental measurement ($-13° \pm 7°$). Note that using the low Reynolds number approximation (equation 5, and using in calculations its Fourier transform that can be found in Yang and Leal 1991), instead of the large Reynolds number approximation (Eq. 4), provides $\Delta\phi = -22°$. We conclude that we are in an intermediate range where low- and high-Reynolds predictions converge. The predicted oscillation amplitude is $\varepsilon/\varepsilon' = 0.72$, also higher than measured values (0.35). These predictions show the limits of the far-field approximation, especially for the secondary Bjerknes force F_B which mainly determines the amplitude of translation.

Note that at first order the secondary Bjerknes forces is alternately attractive and repulsive. However, averaging Eq. 3 over time gives a second order force $\langle F_B \rangle = -(9/16)\rho_l V_B \varepsilon^2 a\omega^2$. Eventually, on an average, the bubble is attracted by its own image! This attractive effect is evidenced in experiments: the center of mass moves closer to the wall when the sound amplitude is increased. It is consistent with the prediction that two bubbles in the bulk, oscillating in phase, experience an attractive secondary Bjerknes force (Leighton 1994). The previous expression is valid only in the far-field limit: the influence of the near-field interaction on the average force can be found in Doinikov and Zavtrak (1995). A detailed calculation of average force including the influence of viscous effects around clean bubbles was also presented in Doinikov (2002).

As a conclusion, these observations and the present theoretical description of the motion validate the assumption of a phase shift between volumetric and translational oscillations of a bubble in contact with a wall, assumption that was necessary to account for the steady acoustic streaming around bubbles that we study in the next section.

4 Resolved acoustic streaming

The primary oscillations of the bubble wall drive oscillations of the liquid. In this section we present direct observations of the liquid motion, using a tracer particle (here a tiny dust particle, a few micrometers in diameter). The particle is small compared with the bubble size that provides the characteristic lengthscale of the flow. A fast-framing image sequence allows following the tracer particle motion during an ultrasound cycle, together with the bubble radius (see Fig. 6). Since the view is along the axis of translation (z), only the radial oscillation can be captured.

The bubble radius R is measured on the sequence of images, together with the distance r_{P} of the particle center to the bubble center projected onto the plane of view. Superimposed on the oscillation, a tiny drift motion of the particle is apparent, amounting to about 0.063 μm/cycle. Note that here we only measure the component of motion parallel to the plane (see Fig. 7). The drift corresponds to a significant translation speed of about 8.7 mm/s, covering the bubble radius in about 2 ms.

Average steady-streaming velocities around the bubble were reported (Marmottant and Hilgenfeldt 2003), but a quantitative prediction of the velocity magnitudes was not possible, in the absence of detailed measurements of the primary oscillations of the bubble and particle, and in particular of the phase shift $\Delta\phi$. The steady flow was interpreted as acoustic streaming, a non-linear response of the flow caused by viscous attenuation effects within the thin oscillatory boundary

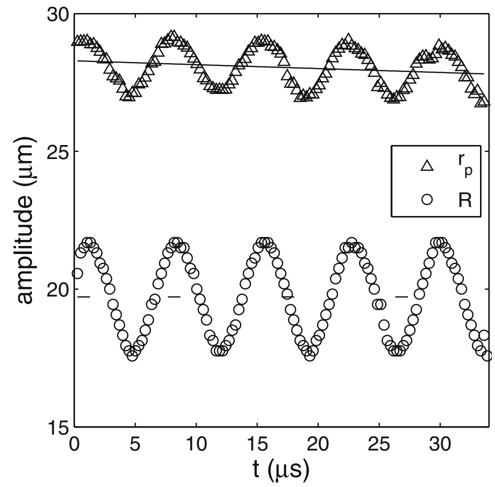

Fig. 7 Resolved particle distance r_{P} and bubble radius R (data from image sequence, see Fig. 6). The tracer particle position exhibits a drift cycle after cycle, resulting in the steady acoustic streaming

layers that surround the bubble wall. Assuming combined translation and radial oscillations, the characteristic velocity of acoustic streaming is $u_{\mathrm{s}} = \varepsilon\varepsilon' a\omega \sin \Delta\phi$, a quadratic non-linear response, expressed here for small amplitudes of vibration ($\varepsilon \ll 1$ and $\varepsilon' \ll 1$). The assumption of combined oscillations is now confirmed by the observations reported in the previous section.

Computation shows that the general case of a steady-streaming flow near a wall can be described in its far field as a superposition of flow singularities, including those of point force and dipole type. The streamlines are closed loops around stagnation points distributed along a circle above the bubble, creating a toroidal vortex (see streamines in Fig. 8). The particle imaged here is therefore circulating along one of these orbits. In Fig. 8, we add lines of constant flow speed (dotted), computed from the analytical expressions in Marmottant and Hilgenfeldt (2003), demonstrating that the speed peaks close to the bubble boundary at values of about u_{s}, and decays rapidly away from the wall.

From the oscillation amplitude $\varepsilon' = 0.1$ measured from the perpendicular view, and using the measurements from the side view to estimate ε/ε' and $\sin \Delta\phi$ (performed at a slightly different frequency), we obtain a

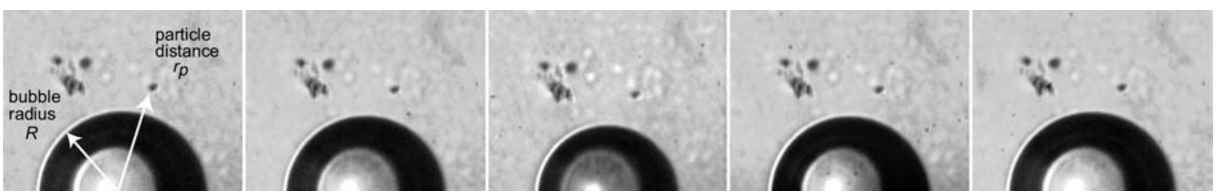

Fig. 6 Bubble (20 μm in radius) and particle, *bottom view* (perpendicular to the glass wall). An agglomerate of particles, too large to be considered as a tracer is also present in the field of view. Images were extracted (one every eight images) from a sequence recorded at the rate of 3,800,000 frames per second, for an ultrasound excitation of 140 kHz

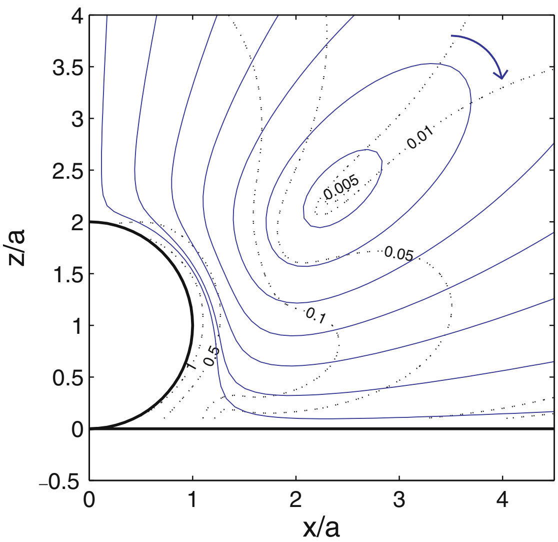

Fig. 8 Side view of the theoretical streamlines around the bubble (*solid lines*) and isocontours of the velocity magnitude in units of $u_s = \varepsilon\varepsilon' a\omega \sin \Delta\phi$ (*dotted lines*)

characteristic streaming velocity u_s of 6 mm/s. It provides a correct order of magnitude when compared with the tracer velocity component measured directly on the resolved sequence (8.7 mm/s), even if we do not know the direction and exact position of the streamline on which the tracer is located.

5 Conclusions

We reported fast-framing observations that provide evidence of an oscillatory translation of the bubble superimposed on the radius oscillation. We showed that this strong translation, comparable in magnitude with the radius oscillation, is caused by the proximity of the wall, acting like an image bubble. The phase shift between these oscillations is created by drag forces. The acoustic streaming of the fluid induced by the bubble appears as a drift of the tracer particle position in a time-resolved image sequence.

In conclusion, the adsorbed oscillating bubble acts as a micron-scale liquid pump propelling liquid with the characteristic velocity $u = \varepsilon'^2(\varepsilon/\varepsilon')a\omega \sin \Delta\phi$, proportional to the square of the vibration amplitude ε'. The efficiency of this pump is the greatest when fixed to the wall since it is the closest to the wall (maximizing ε/ε'), and the efficiency proves to be enhanced in viscous media, triggering a larger phase shift $\Delta\phi$ between oscillation and translation. Note that this is in contrast to the traditional streaming flow scenario, where the streaming velocity is independent of the value of viscosity.

Acknowledgments We would like to thank Stefan Luther for fruitful discussions on image analysis. The work is part of the research program of FOM, which is financially supported by NWO.

References

Brennen CE (1995) Cavitation and bubble dynamics. Oxford University Press, Oxford

Chin CT, Lancée C, Borsboom J, Mastik F, Frijlink M, de Jong N, Versluis M, Lohse D (2003) Brandaris 128: a digital 25 million frames per second camera with 128 highly sensitive frames. Rev Sci Instrum 74:5026–5034

Doinikov AA (2002) Viscous effects on the interaction force between two small gas bubbles in a weak acoustic field. J Acoust Soc Am 111:1602–1609

Doinikov AA, Zavtrak ST (1995) On the mutual interaction of two gas bubbles in a sound field. Phys Fluids 7:1923–1930

van der Geld CWM (2002) On the motion of a spherical bubble deforming near a plane wall. J Eng Math 42:91–118

van der Geld CWM (2004) Prediction of dynamic contact angle histories of a bubble growing at a wall. Int J Heat Fluid Flow 25:74–80

Klibanov AL (2002) Ultrasound contrast agents: development of the field and current status. Top Curr Chem 222:73–106

Leighton TG (1994) The acoustic bubble. Academic, London

Longuet-Higgins MS (1997). Particle drift near an oscillating bubble. Proc Roy Soc Lond A 453:1551–1568

Longuet-Higgins MS (1998) Viscous streaming from an oscillating spherical bubble. Proc R Soc Lond A 454:725–742

Magnaudet J (2003) Small inertial effects on a spherical bubble, drop or particle moving near a wall in a time-dependent linear flow. J Fluid Mech 485:115–142

Magnaudet J, Eames I (2000) The motion of high-Reynolds-number bubbles in inhomogenenous flows. Annu Rev Fluid Mech 32:659–708

Magnaudet J, Legendre D (1998) The viscous drag force on a spherical bubble with time-dependent radius. Phys Fluids 10:550–554

Marmottant P, Hilgenfeldt S (2003) Controlled vesicle deformation and lysis by single oscillating bubbles. Nature 423:153–156

Miller DL, Quddus J (2000) Sonoporation of monolayer cells by diagnostic ultrasound activation of contrast-agent gas bodies. Ultrasound Med Biol 26:661–667

Pelekasis NA, Gaki A, Doinikov A, Tsamopoulos JA (2004) Secondary Bjerknes forces between two bubbles and the phenomenon of acoustic streamers. J Fluid Mech 500:313–347

Tachibana K, Uchida T, Ogawa K, Yamashita N, Tamura K (1999) Induction of cell membrane porosity by ultrasound. Lancet 353:1409

Takemura F, Magnaudet J (2003) The transverse force on clean and contaminated bubbles rising near a vertical wall at moderate Reynolds number. J Fluid Mech 495:235–253

Ward M, Wu J, Chiu JF (2000) Experimental study of the effects of OPTISON® concentration on sonoporation in vitro. Ultrasound Med Biol 26:1169–1175

Yang SM, Leal LG (1991) A note on memory-integral contributions to the force on an accelerating spherical drop at low Reynolds number. Phys Fluids A 3:1822–1824